ELSEVIER

NeuroImage

www.elsevier.com/locate/ynimg
NeuroImage 25 (2005) 491–501

The many faces of the gamma band response to complex visual stimuli

Jean-Philippe Lachaux,[a,b,*] Nathalie George,[a] Catherine Tallon-Baudry,[a] Jacques Martinerie,[a] Laurent Hugueville,[a] Lorella Minotti,[c] Philippe Kahane,[c] and Bernard Renault[a]

[a]*Laboratoire de Neurosciences Cognitives et Imagerie Cérébrale (LENA), CNRS URA 654, Hôpital de La Salpêtrière, 47 Bd de l'Hôpital, 75651 Paris cedex 13 Paris*
[b]*U280, Mental Processes and Brain Activation, 151 Cours Albert Thomas, 69003, Lyon, France*
[c]*Department of Neurology and INSERM 318 Research Unit, Grenoble Hospital, 38000 Grenoble, France*

Received 11 May 2004; revised 25 November 2004; accepted 30 November 2004
Available online 26 January 2005

While much is known about the functional architecture of the visual system, little is known about its large-scale dynamics during perception. This study describes this dynamics with a high spatial, temporal and spectral resolution. We recorded depth EEG of epileptic patients performing a face detection task and found that the stimuli induced strong modulations in the gamma band (40 Hz to 200 Hz) in selective occipital, parietal and temporal sites, in particular the fusiform gyrus, the lateral occipital gyrus and the intra-parietal sulcus. Occipito-temporal sites were the first to be activated, closely followed by the parietal sites, while portions of the primary visual cortex seemed to deactivate temporarily. Some of those effects were found to be correlated across distant sites, suggesting that a coordinated balance between regional gamma activations and deactivations could be involved during visual perception.

Keywords: Induced gamma response; Beta band; Event-related potentials; Functional connectivity; Face perception; Intracranial EEG

Introduction

This paper investigates directly with intracerebral recordings in humans the first couple of hundred of milliseconds of visual perception, when a meaningful visual object pops out effortlessly into conscious perception after rapid integration of distributed visual features.

Many functional imaging studies have already mapped out major components of the large-scale networks involved in object perception. Face perception, for instance, involves a core system that includes the lateral fusiform gyrus, the superior temporal sulcus and the lateral occipital gyrus (see (Haxby et al., 2000) for a review). Yet, functional Magnetic Resonance Imaging (fMRI) and Positron Emission Tomography (PET) lack the temporal resolution necessary to capture the details of the fast neural dynamics underlying perception. A couple of influential studies have used human intracranial EEG recordings to provide a spatially and temporally resolved investigation of the face perception system (Allison et al., 1994a,b, 1999; Halgren et al., 1994a,b; McCarthy et al., 1999; Puce et al., 1999); but their scope was limited to the electrical potentials evoked by (i.e., phase-locked to) visual stimuli or to a limited view of the EEG spectrum (Klopp et al., 1999).

A complete study of the electrophysiological response to visual stimuli should describe at the intracerebral level all its multidimensional components; that is, not only the event-related potentials (ERP), but also the EEG spectral modulations that disappear in the averaging procedure used to compute ERPs. Indeed, numerous studies, both in humans and animals, have come to support the hypothesis that the integration of visual features into perceived objects involves such modulations above 40 Hz (i.e., in the gamma band) (Gray, 1999; Singer, 1999). In particular, the perception of meaningful objects in humans is simultaneous with a well-documented increase of power in the scalp EEG in the gamma band: the induced gamma response (so called because it is not phase-locked to the object presentation) (Rodriguez et al., 1999; Tallon-Baudry and Bertrand, 1999). But despite recent developments (Klopp et al., 1999, 2000; Lachaux et al., 2000), the neural sources of this induced gamma response in humans are totally unknown.

This paper revolves around two general questions: (a) what are the neural sources of the gamma responses induced during the perception of complex objects? (b) What is the functional significance of the induced gamma response for object perception and how does it coincide with the network already mapped with functional imaging?

We addressed those two questions using a particular face detection task that yielded clear induced gamma responses at the scalp EEG level (Rodriguez et al., 1999). We recorded depth-EEG from four implanted epileptic patients and looked for spectral

* Corresponding author. U280, Mental Processes and Brain Activation, 151 Cours Albert Thomas, 69003, Lyon, France. Fax: +33 4 72 68 19 02.
E-mail address: lachaux@lyon.inserm.fr (J.-P. Lachaux).
Available online on ScienceDirect (www.sciencedirect.com).

1053-8119/$ - see front matter © 2004 Elsevier Inc. All rights reserved.
doi:10.1016/j.neuroimage.2004.11.052

changes induced by the face presentations in a wide frequency range (1–200 Hz).

Methods

Subjects

All four patients (Pt1, a 31-year-old female; Pt2, a 27-year-old male; Pt3, a 28-year-old male. Pt4, a 27-year-old female) suffered from drug-resistant partial epilepsy and were candidates for surgery. MRI was normal in three patients (Pt1-2-3) and showed left parietal atrophy in the fourth patient (Pt4). Because the location of the epileptic focus could not be identified using noninvasive methods, the patients underwent intracerebral recordings by means of stereotactically implanted multilead depth electrodes, on the basis of which the epileptogenic zone proved to be right occipito-temporal in patient Pt1, left occipital in patient Pt2, right occipito-parieto-temporal in patient Pt3, and bilateral occipito-parieto-temporal in patient Pt4. The selection of the sites to implant was made entirely for clinical purposes with no reference to the present experimental protocol. However, patients who entered this protocol were selected because their implantation sampled the occipito-parieto-temporal lobes. The patients performed the task 4 days after the implantation of the electrodes and had previously given their informed consent to participate in the experiment.

Electrode implantation

Eleven to 14 semi-rigid electrodes were implanted per patient, in cortical areas which varied depending on the suspected origin of their seizures (Fig. 3). Each electrode had a diameter of 0.8 mm and comprised 10 or 15 leads of 2 mm length, 1.5 mm apart (Dixi, Besançon, France), depending on the target region. Therefore, various mesial and lateral cortical areas were evaluated, including sulcal cortex. For each patient, we measured the coordinates of all the electrode contacts on his stereotactic scheme, in the Talairach coordinates system. After a linear scale adjustment (to correct for size differences between the patient's brain and the brain in the Talairach atlas), those coordinates were used to localize anatomically the contacts using the proportional atlas of Talairach and Tournoux. Those anatomical locations were confirmed via an additional procedure that allowed to visualize directly the positions of the electrodes contact sites on the patient's MRI (this procedure consisted in the computer-assisted matching of the post-implantation CT-scan (showing the contact sites) with a pre-implantation 3-D MRI (VOXIM R, IVS. Solutions, Germany)).

Paradigm

The experimental protocol was the same one as in our previous studies (George et al., 1997; Rodriguez et al., 1999). In brief, Mooney faces (Mooney, 1956) were presented for 200 ms randomly in an upright or inverted position in a total of 640 trials (320 and 320). 320 trials were presented in a first series of four blocks (each with a random mixture of 40 upright and 40 inverted faces) followed by the same 320 trials in a different order (in fact, the same four blocks, but in a different order). The interval between two consecutive stimulus onsets varied randomly between 1500 ms and 2500 ms; in between stimuli, the screen remained black. Stimuli were presented to the participants on a 17″ computer screen. The stimulus dimensions were 8 cm × 4.5 cm, subtending a visual angle of approximately 2 × 1° at the 200 cm viewing distance. The patients were instructed to fixate the center of the screen and, after each stimulus, to report on their first impression: that is, whether they had immediately perceived a face or not, whatever its orientation. They had to respond as fast as possible using two response buttons mounted on a mouse held in their right hand. They had to press a button with their right middle finger if they had seen a face, or a second button with their right index finger if they had not seen it.

Recording and data analysis

Intracerebral recordings were conducted using an audio-video-EEG monitoring system (Micromed, Treviso, Italy), which allowed the simultaneous recording of 63 depth-EEG channels sampled at 512 Hz [0.1–200 Hz band width]. Stimuli were sorted into four categories prior to analysis: upright Mooney figures perceived as faces (UY), upright Mooney figures not perceived as faces (UN), inverted figures perceived as faces (DY), and inverted figures not perceived as faces (DN) (see Table 1). Recording sites showing clear epileptiform activities were excluded from the analysis, and among the remaining sites, monopolar and bipolar data were systematically inspected, both raw and high-pass filtered (above 15 Hz), for any sign of epileptiform artifact. Any trial showing epileptic spikes in any of those traces was discarded. We also monitored the electrooculogram to discard trials with eye movements; however, since the stimuli were small and presented foveally, the patients really had to maintain their gaze centered in order to do the task.

Time-frequency analysis

For each single trial, bipolar derivations computed between adjacent electrode contacts were analyzed in the time-frequency domain by convolution with complex Gaussian Morlet's wave-

Table 1
Behavioral performance of the patients and number of analyzed trials per class of events

Patient	Stimulus/ response	No. of responses (%)	No. of analyzed trials	Mean RT (ms)	Standard RT (ms)
Pt1	UY	233/320 (73%)	87	691	167
Pt1	UN	45/320 (14%)	12	969	263
Pt1	DY	45/320 (14%)	28	1028	282
Pt1	DN	231/320 (72%)	153	1035	249
Pt2	UY	268/320 (83%)	139	728	144
Pt2	UN	51/320 (16%)	25	900	167
Pt2	DY	129/320 (40%)	87	783	167
Pt2	DN	190/320 (59%)	134	923	165
Pt3	UY	235/320 (73%)	100	687	146
Pt3	UN	85/320 (27%)	33	806	143
Pt3	DY	140/320 (44%)	115	795	198
Pt3	DN	180/320 (56%)	156	832	145
Pt4	UY	296/320 (92%)	73	600	166
Pt4	UN	21/320 (7%)	8	881	236
Pt4	DY	195/320 (61%)	127	657	193
Pt4	DN	119/320 (37%)	81	878	181

Events classes: UY (perceived upright faces), UN (not perceived upright faces), DY (perceived inverted faces), DN (not perceived inverted faces).

lets (Tallon-Baudry et al., 1997), thus providing a time-frequency power map $P(t, f) = |w(t, f) \times s(t)|^2$, where $w(t, f)$ was for each time t and frequency f a complex Morlet's wavelet $w(t, f) = A \exp(-t^2/2\sigma_t^2).\exp(2i\pi ft)$, with $A = (\sigma_t\sqrt{\pi})^{-1/2}$ and $\sigma_t = 1/(2\pi\sigma_f)$ and σ_f a function of the frequency f: $\sigma_f = f/7$.

Normalized time-frequency maps were computed for each bipolar derivation, for visualization purpose. This normalization was done separately for each frequency, and consisted in (a) subtracting the mean power during a [−500 ms:−100 ms] prestimulus baseline and (b) dividing by the standard deviation of the power during this same baseline.

To determine whether oscillatory responses were phase-locked to the stimulus, we computed time-frequency maps of phase-locking factors (Tallon-Baudry et al., 1997) and compared the values obtained after the stimulation with the values during the baseline.

Significant spectral modulations caused by the stimuli were detected using a Wilcoxon non-parametric test that compared across the trials, the total energy in a given time-frequency tile, with that of a tile of similar frequency extent, but covering a prestimulus baseline period [from −500 ms to −100 ms] (typically in this study, the frequency extent of the tiles was 50–200 Hz to detect gamma responses). Significant responses were defined by a P value less than 0.001.

Comparison between pairs of stimulus/response combinations (e.g., UY vs. DN) were done via a Kruskal–Wallis non-parametric analysis (in the text: KW) applied to the raw time-frequency values of energy, on a set of time-frequency tiles [100 ms × 8 Hz] covering a [0:1000 ms] × [1:200 Hz] domain (one test per tile comparing the values obtained for all the trials in the two conditions).

EEG signals were evaluated with the software package for electrophysiological analysis (ELAN-Pack) developed in the INSERM U280 laboratory.

Phase and amplitude correlations across recording sites.

We used a wavelet-based estimation of synchrony to test for possible phase-locking between certain spectral components of the response (beta and gamma responses) (Lachaux et al., 2002). In short, the analysis extracts the time course of the instantaneous phase-difference between two signals in each trial around a frequency of interest (as computed using Morlet's wavelets), and estimates the circular variance of that difference on a sliding window the duration of which depends on the analyzed frequency (8 cycles of oscillations). This circular variance is a time-varying measure of phase-locking between 0 (no phase-locking) and 1 (complete synchrony) which is averaged across trials to provide an average measure of synchrony between signals.

We also tested for possible cross-site correlations between the energy of well-defined induced gamma responses. This was done by defining for each site a time-frequency region of interest (TFROI), centered on the induced gamma response in this site, and then computing a Spearman rank correlation coefficient between the series of energy values obtained for each one of two sites within their TFROI across the trials (Lachaux et al., 2003).

Results

The performance of the patients was similar to that observed in normal subjects (George et al., 1997; Rodriguez et al., 1999): they mostly perceived faces when they were presented upside up, and except for Pt4, they did not perceive the face in the majority of the inverted figures (Table 1). Data were only analyzed for upright stimuli perceived as faces (UY), downward stimuli perceived as faces (DY) and downward stimuli not perceived as faces (DN), that is, the classes of events for which the number of trials after artifact rejection was sufficient (see Methods section for a description of the rejection procedure). Since much emphasis has already been put in previous studies on the (mostly low-frequency) potentials evoked by faces, either from surface or intracranial EEG, the result section focuses mainly on the frequency components of the electrophysiological response that do not appear in the evoked potential.

Gamma band responses induced by the visual stimuli

In a limited, but specific set of recording sites (see Table 2), the presentation of the Mooney figures produced for all stimulus types a focal increase of energy above 40 Hz significantly greater than the average gamma energy level in the baseline (Fig. 1), (Wilcoxon vs. baseline, $P < 0.001$ for each site). Except in one site in Brodmann Area 19 (s′12s′13, Pt2, illustrated in Fig. 2), those gamma oscillations were not phase-locked to the stimulus that initiated them (phase-locking factor: comparison with the prestimulus baseline).

In our posterior cortical sampling (Fig. 3), those induced gamma responses were distributed consistently around two structures, the fusiform gyrus and the intraparietal sulcus, together with distributed sites along the ventral visual pathway (see Fig. 2 for representative examples).

Responses along the ventral visual pathway

All classes of stimuli activated a broad portion of the fusiform gyrus, in a fairly typical manner (Fig. 1), causing after 200 ms an abrupt energy increase above 40 Hz, and up to 200 Hz, which focused progressively around the beta band (in a 'wing-like' shape) after 500 to 600 ms (that is, before the motor response). After the initial burst, the gamma modulation decreased almost linearly in amplitude (see Fig. 3). These gamma responses co-occurred with a strong energy drop below 30 Hz that ended around 600 ms, at which time there was a clear energy rebound in the beta band. This rebound was clearly visible in the raw traces (see Fig. 4). It was synchronous across several sites within the fusiform gyrus and with the intraparietal sulcus (the synchrony level, though, was the same for perceived vs. non-perceived faces).

Specific recording sites within the ventral occipito-temporal region showed sensitivity to face perception (and perceived faces elicited the strongest responses, as detailed below). Let us review those effects on the basis of the patient's anatomy. In one of those sites (Pt3, e1e2, right fusiform gyrus, see Fig. 5), the gamma response was stronger for the UY than for DN stimuli between 400 ms and 800 ms (Pt3, e1e2, Kruskal–Wallis (KW) $P < 0.001$). Interestingly, at the frequency where the effect was the strongest (80 Hz), the response was also significantly stronger for UY than for DY figures (KW $P > 0.001$), but this difference lasted only from 400 ms to 500 ms, after which the response to the DY faces became significantly stronger than the one to the DN stimuli (DY > DN $P > 0.001$, from 500 ms to 800 ms, that is the reaction time to DN stimuli); as if the processing of DY stimuli, as faces, was delayed by 100 ms compared to UY stimuli.

Table 2
Talairach coordinates of each site with induced gamma responses to Mooney stimuli, together with observed significant differences between classes of events (ns = not significant)

Patient ID	Bipole	Talairach *x*, *y*, *z*	Anatomical localization	UY > DN	UY > DY	DY > DN	Electrically-induced symptoms*
Pt1	e1–2	+25, −43, −13	R fusiform gyrus (next to the T4–T5 sulcus, BA37)	ns	n/a	n/a	none
	e11–12	+63, −43, −13	R inferior temporal gyrus (BA37)	500–750 ms	n/a	n/a	none
	p7–8	+30, −62, +37	Depth of the R intraparietal sulcus (BA7)	250–850 ms	n/a	n/a	Simple visual hallucination in the L upper visual field (3 mA)
	s8–9	+37, −76, +17	Mid occipital gyrus (lateral aspect, BA19)	ns	n/a	n/a	none
	o1–2	+7, −76, +6	Inferior bank of the R calcarinian fissure (BA17)	ns	n/a	n/a	Simple visual hallucination in the L upper visual field (0.6 mA)
	o12–13	+48, −76, +6	Mid occipital gyrus (lateral aspect, BA 19)	250–600 ms	n/a	n/a	none
	f4–5	+29, −55, −2	R fusiform gyrus (next to the T4–T5 sulcus, BA37)	ns	n/a	n/a	none
Pt2	e4–5	−39, −66, −7	L fusiform gyrus (BA19)	ns	ns	ns	none
	e7–8	−51, −66, −7	L inferior temporal gyrus (next to the T3–T4 sulcus, BA37)	250–750 ms	250–750 ms	750–1000 ms	none
	o1–2	−8, −84, +4	Inferior bank of the L calcarinian fissure (BA17)	ns	ns	ns	Simple visual hallucination in the R upper visual field (1 mA)
	o7–8	−30, −84, +4	Depth of the L mid occipital sulcus (BA18)	ns	ns	ns	none
	o11–12	−45, −84, +4	L inferior occipital gyrus (lateral aspect, BA18)	ns	ns	ns	none
	s12–13	−45, −74, +18	L mid occipital gyrus (lateral aspect, BA19)	ns	ns	ns	Counterclockwise rotatory simple visual hallucination (2 mA)
	w8–9	−31, −68, +24	Depth of the L intraparietal sulcus (BA7/19)	ns	DY > UY. 500–1000 ms	500–1000 ms	none
Pt3	w7–8	+28, −67, +25	Depth of the R intraparietal sulcus (BA7/19)	ns	ns	ns	none
	o8–9	+31, −69, +16	Depth of the R intraparietal sulcus (BA7/19)	ns	ns	ns	none
	f7–8	+41, −56, −8	R fusiform gyrus (BA37)	ns	ns	ns	Visual illusion in the upper L visual field + head spinning (0.8 mA)
	f8–9	+44, −56, −8	R fusiform gyrus (BA37)	ns	ns	ns	none
	e1–2	+36, −38, −15	R fusiform gyrus (BA36/37)	400–800 ms	400–500 ms	500–800 ms	none

Table 2 (*continued*)

Patient ID	Bipole	Talairach *x*, *y*, *z*	Anatomical localization	UY > DN	UY > DY	DY > DN	Electrically-induced symptoms*
Pt4	o1–2	−8, −57, 11	Inferior bank of the L calcarinian fissure (BA17)	ns	ns	ns	na (but for o2–3, 0,2 mA: simple visual hallucination in the R upper visual field)
	f5–6	−35, −40, 3	L fusiform gyrus (depth of the T4–T5 sulcus, BA37)	ns	ns	ns	none

R/L: right/left; * bipolar stimulation (pulse width: 1 ms, duration: 5 s) were delivered using a constant current rectangular pulse generator (Micromed, Treviso, Italy) according to our standard clinical practice; we took into account only the symptoms elicited at the lowest intensity; we excluded the stimulation which had elicited epileptic symptoms and clinical signs associated with an induced afterdischarge.

In another patient (Pt2), a site situated more laterally in the occipital region also yielded some responsiveness to face perception (Pt2, e7e8, left inferior temporal gyrus, see Fig. 5): there, gamma responses were stronger for UY than DN from 250 ms to 1000 ms (KW, $P < 0.001$) and for UY than DY from 250 ms to 750 ms (KW < 0.001), after which DY responses were greater than DN responses (until 1000 ms, KW < 0.001), again, it seemed that DY processing mirrored that of DN stimuli, before finally resembling that of UY stimuli. This effect was very localized since for another bipole 1 cm more medial on the same electrode (e4e5, left fusiform gyrus), the gamma response was the same for all event types. Interestingly, both sites with face superiority effects (e1e2 in Pt3 and e7e8 in Pt2) were located in the broad ventral occipito-temporal region often found to be selective to faces (Grill-Spector, 2003; Kanwisher et al., 1997). Further down the ventral stream, in yet another patient (Pt1, e11e12, right inferior temporal gyrus), we observed a superiority effect for UY events over DN, but this one came later than in the more posterior sites, between 500 and 750 ms. Unfortunately, there were two few DY events to include this condition in the analysis for this patient

Face superiority effects were also observed in the Lateral Occipital gyrus in patient Pt1 (Fig. 5). (Pt1: o12o13, right lateral occipital gyrus) and the gamma response was also stronger for UY than DN at similar latencies (KW, $P < 0.001$ from 250 ms to 600 ms). The location of this site also corresponded with a region found to be selective to faces with fMRI (Grill-Spector, 2003). In a position symmetrical in the left hemisphere, but in patient Pt2, (Pt2, o11 o12, left inferior occipital gyrus), we found a strong gamma response with a similar time course, but there were no differences between event types. A similar effect was observed slightly more medially, on the same electrode (Pt2, o7o8, left middle occipital sulcus), although with a faster decay after 400 ms.

Responses in the intraparietal sulcus

Stimuli also ignited the dorsal visual pathway, mostly along the intraparietal sulcus. The parietal responses lacked the initial, abrupt, energy burst observed in the fusiform gyrus and were typically later (see Fig. 3). In this cortical sampling, the latency of this parietal gamma response also increased with the distance to the occipital lobe. We observed a difference between conditions in two sites: first, in the most anterior recording site of the right intraparietal sulcus, in the vicinity of the Lateral Intraparietal Area (LIP) that is part of the parietal attentional system (Rushworth et al., 2001). There, UY generated a stronger gamma response for a long 250 ms to 850 ms interval (Pt1, p7p8, right intraparietal sulcus, KW, $P < 0.001$), which could be explained by an 'attention-grabbing' effect of perceived faces (or alternatively, by the triggering of reflex eye movements, see Discussion). In another part of the intraparietal sulcus (Pt2, w8w9) that has been found to be involved in mental rotation (Gauthier et al., 2002), the gamma response was stronger for DY stimuli than for UY and DN stimuli

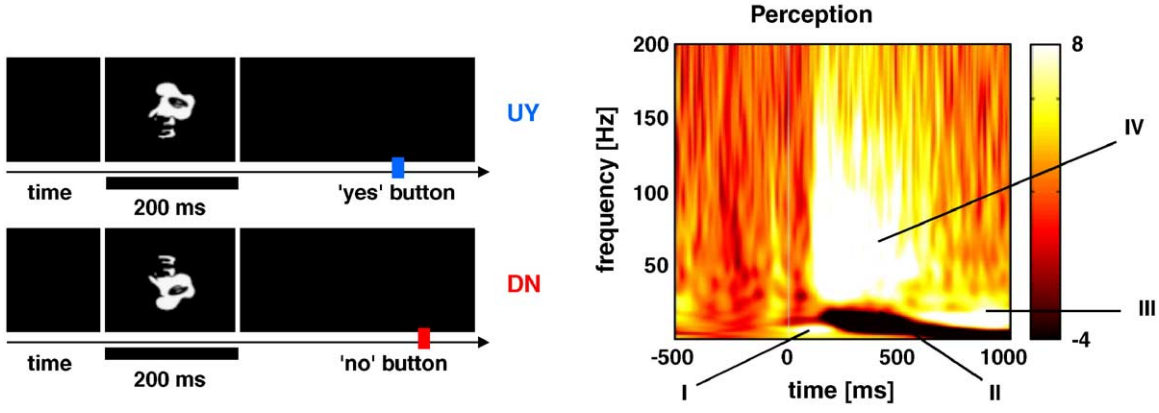

Fig. 1. Typical time-frequency response to Mooney stimuli in the fusiform gyrus. After a 200-ms presentation of the stimulus, the patients had to respond whether a face popped out in the picture, or not. The normalized time-frequency map displays the augmentation in power relative to the [−500:−100 ms] baseline (in standard deviations). It shows four typical components, (I) the trace of the low-frequency evoked-potential; (II) the event-related desynchronization in the alpha and beta bands; (III) the late rebound in the beta band; (IV) the induced gamma response with a 'wing-like' profile: the fastest frequency components of this response decay faster than the slowest ones.

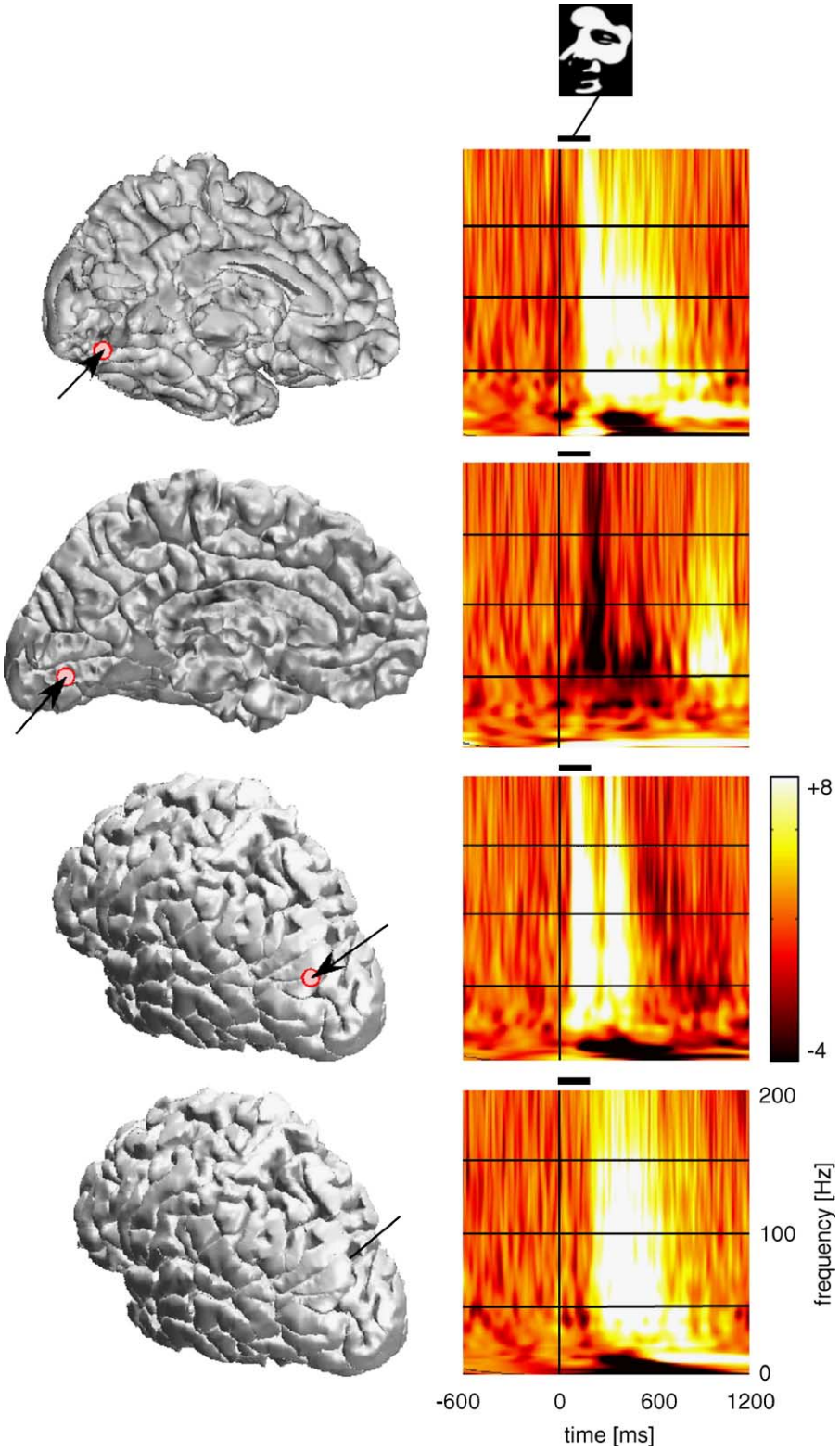

Fig. 2. The many faces of the gamma band response. Four typical examples of Time-Frequency modulations by face stimuli. In this patient (Pt 2), those four bipoles recorded from (from top to bottom) the fusiform gyrus (e4e5), the primary visual cortex (o1o2), the median part of the lateral occipital gyrus (BA19, s12s13) and the intraparietal sulcus (w8w9) in the left hemisphere. The TF modulation map displays the augmentation in power relative to the [−500:−100 ms] baseline (in standard deviations). When the Primary Visual Cortex bipole was stimulated at 50 Hz, the patient perceived a flash near the center of its visual field. In BA19 (second map from the bottom), we clearly see an on and off response to the stimulation, separated by the duration of the presentation (200 ms). Those on and off responses were phase-locked to the stimulus.

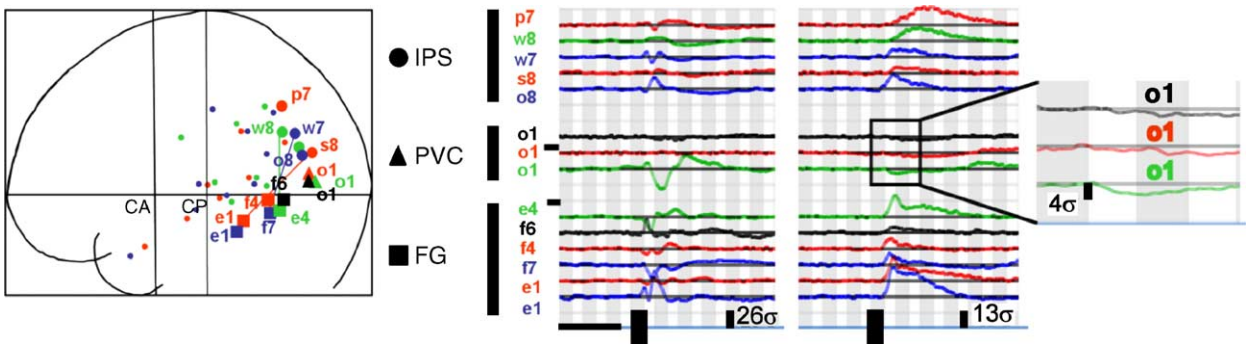

Fig. 3. Spatio-temporal organization of the induced gamma responses to face stimuli. Left graph shows the entry sites of the electrodes implanted in all four patients (patients are color coded). Large symbols indicate sites where induced gamma responses were observed. Lines link parietal and temporal sites which gamma responses were correlated in amplitude across the trials. Labeled Bipoles were fusiform gyrus (FG, squares), primary visual cortex (PVC, triangles) and intraparietal sulcus sites (IPS, circles). For those sites, the right graphs display the time course of the evoked potentials and the energy in the [50–150 Hz] gamma band, both normalized (z score) relative to the same [−500 ms:−100 ms] prestimulus baseline. Sites in the primary visual cortex have been zoomed in for a better visualization of the gamma 'deactivation'.

from 500 ms to 1000 ms. In fact, this activation slightly anticipated the gamma response to DY stimuli in the Fusiform Face Area. Interestingly, DY stimuli were the only one that actually represented inverted faces for the patient, and may therefore have been associated with a mental rotation.

Gamma deactivation in the primary visual cortex

Three of the four patients (Pt1, Pt2, and Pt4) had one pair of contacts passing through the primary visual cortex. There, the energy decreased below the baseline from 200 ms to 500 ms (Wilcoxon, $P < 0.001$) (Fig. 2). This effect, however, was not significantly different between stimulus categories; that is, in this time interval, the energy in the gamma band was not significantly different between classes of events (KW comparison).

Correlations between the ventral and dorsal gamma responses

We systematically tested for possible phase-locking effects in the gamma band between all our recording sites (in the form of significant synchrony increases or decreases relative to the baseline), but we found none; thus, such synchrony effects appeared to be restricted to the beta range in our data set, at this level of spatial resolution. We then tested, in the gamma band, for possible cross-trial correlations between the energy (and not the phase) of the induced responses. We found several instances where the average TF energy between 60 and 90 Hz (calculated during a 200 ms window, specific to each site, covering the most part of its induced response) was correlated between sites. In particular, dorsal and ventral responses appeared to be correlated in several instances: in Pt1, the response in the parietal region mediating attentional processes (p7p8, right intraparietal sulcus) was correlated with the face-sensitive lateral occipital response (o12o13, right middle occipital gyrus) for both types of events (DN (Spearman Ro = 0.387, $P < 0.0001$) and UY (Spearman Ro = 0.179, $P = 0.04$)). Also in Pt1, the intraparietal sulcus (s8s9) was correlated with the fusiform gyrus (e1e2) for UY stimuli (UY, Spearman Ro = 0.22 $P = 0.015$). In Pt2, the other parietal site where inverted faces triggered an increased response, in the left, intraparietal sulcus (w8w9) was correlated with the fusiform gyrus (e4e5) for DN stimuli (Spearman Ro = 0.251, $P = 0.002$). In Pt3, we found the same kind of dorsal–ventral correlation between the right intraparietal sulcus (w7w8) and the right fusiform gyrus (f7f8) (UY, Spearman Ro = 0.19, $P = 0.018$).

Gamma responses vs. evoked potentials

As stated earlier, evoked potentials were not the primary focus of this paper; however, it is worth noting that there were several discrepancies between the effects observed in the gamma range and in the evoked potential. For instance, in Pt1, two sites showed significant face effects in the gamma range but not in the evoked potentials (o12o13, right middle occipital gyrus (Fig. 5), and e11e12, right inferior temporal gyrus). In Pt2, a site in the left inferior temporal gyrus (e7e8) and a site in the left intraparietal sulcus (w8w9) had effects in the gamma range but not in the evoked potentials. The converse was also true, we could observe evoked potentials and face effects in ERPs in regions with no gamma responses: in Pt2, for instance, one site in the middle occipital gyrus (f7f8, Talairach coordinates [−37, −61, 3]), showing no gamma response, displayed a nice evoked potential with a clear negative peak at 170 ms and a positive peak at 250 ms with a much higher amplitude for UY than DN events. The induced gamma responses and the evoked potentials thus clearly appeared to belong to two functionally distinct systems.

Modulations of the alpha and beta bands

As stated earlier, the energy in the alpha and beta bands generally decreased during the induced gamma response (event-related desynchronization, ERD) before rebounding around 600 ms. Interestingly, we did not observe any significant difference between conditions in the amplitude of the ERD in either of those bands, although the strength of the rebound, around the response, may occasionally vary across event types.

Discussion

A coordinated mosaic of induced gamma responses

We gained at least three novel insights into the nature and origin of visually induced high-frequency responses: (a) anatomical

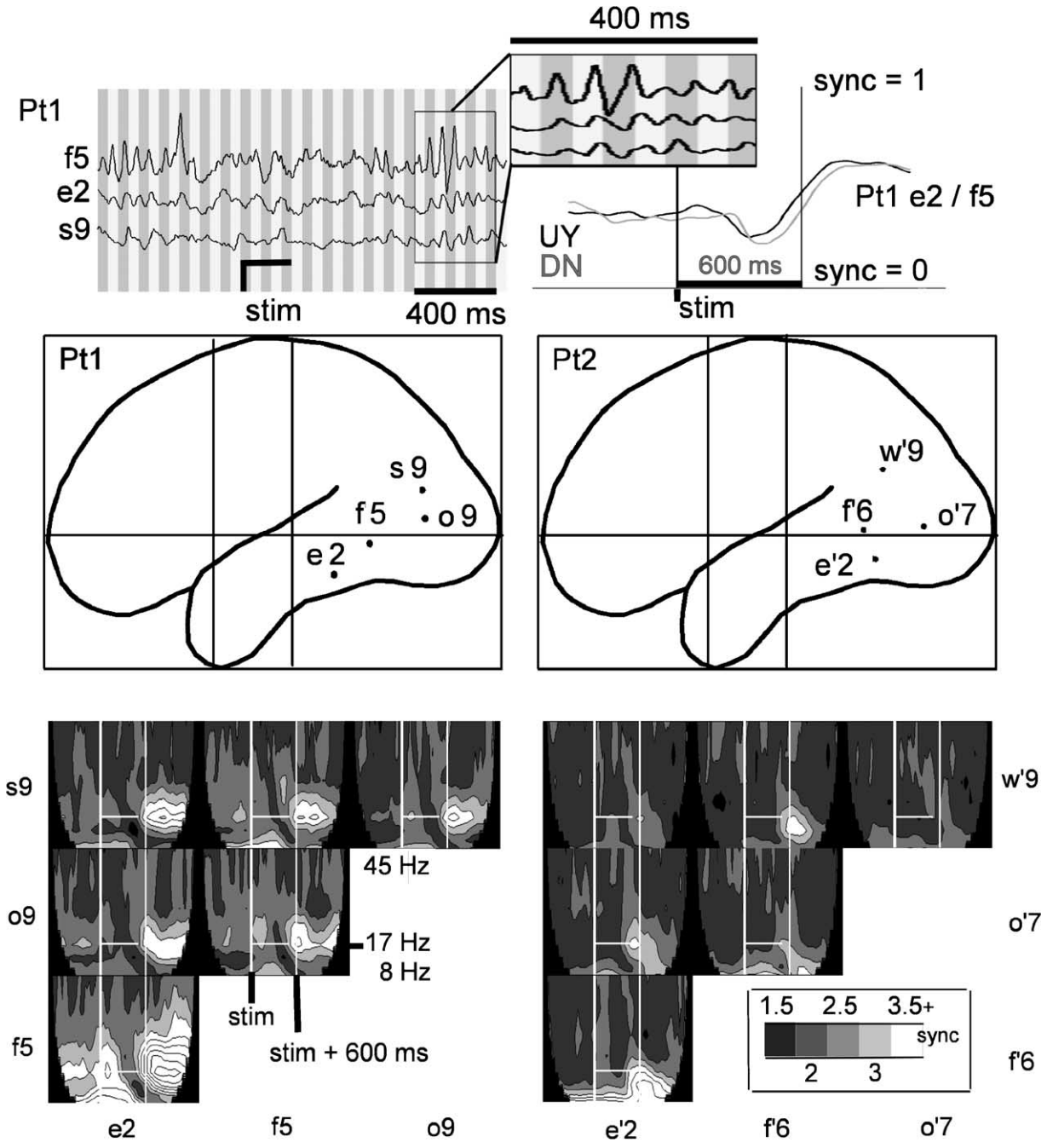

Fig. 4. Synchrony in the beta band. The bottom maps correspond to the TF synchrony maps (obtained with the wavelet coherence technique) averaged across all the UY events between four bipolar recording sites (see Table 2 for the precise anatomical locations). The sites were chosen to illustrate the extent of the synchrony effect. On the brains drawings, the intersection between the horizontal and the anterior vertical line identify the anterior commissure, while the posterior intersection identifies the posterior commissure. An increase of synchrony around 17 Hz after 600 ms can clearly be seen even between distant sites. The top graph on the left displays the raw traces obtained for one particular UY event in three of the sites selected for Pt 1 (e2 and f5 are in the right fusiform gyrus, and s9 is in the middle occipital gyrus). The beta synchronization can be seen in those raw traces 600 ms after the stimulus onset. The right plots correspond to a section of the TF synchrony map (averaged across trials) at 17 Hz between e2 and f5 for the UY and for the DN events, the two plots overlap.

specificity: only a minority of the brain regions that we recorded from did show gamma modulations; (b) diversity: the latency, duration and frequency extent of the gamma response depends strongly on its anatomical origin; (c) cooperation: we found significant correlations between the amplitude of the gamma responses produced in the dorsal and ventral visual pathways, this is a possible indication (although not a proof) that local synchronization in one area may facilitate the synchronization in an other remote area.

In addition, we observed that the gamma band increases co-occurred systematically with decreases in the alpha and beta bands, and sometimes, but not always, with event-related potentials. They were not phase-locked to the stimulus and therefore not filtered components of the evoked potentials (in contrast with the only

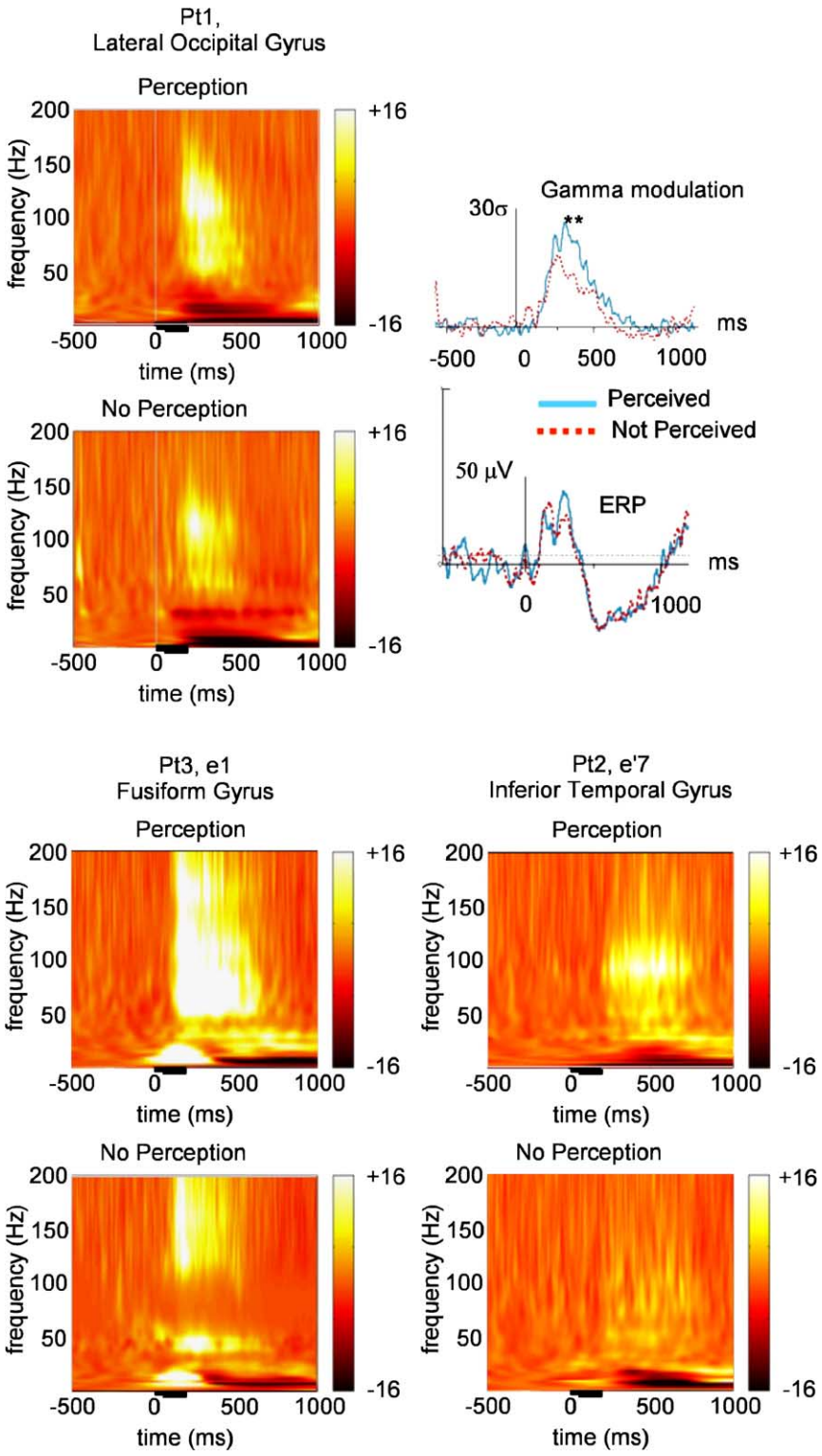

Fig. 5. Face perception effects on the induced gamma response. In the upper part of the figure, the left graphs show for one site in the lateral occipital gyrus (Pt 1, o12o13) the normalized time-frequency maps for both UY and DN events. The right graphs show for the same sites, the time-course of the average modulation of each condition in the [50–150 Hz] frequency range, together with the evoked potential in each condition. The difference between those two conditions is significant in the gamma band (** Kruskal–Wallis, $P < 0.001$) but not for the evoked potentials. In the lower part of the figure, the left (resp. right) maps show for one site in the fusiform gyrus (Pt3, e1e2) (resp. for one site in the inferior temporal gyrus, Pt2, e7e8) the normalized time-frequency maps for both UY and DN events; UY events generate significantly stronger gamma responses than DN events.

other gamma responses observed so far at this level of resolution during the perception of faces (Klopp et al., 1999)). The induced gamma responses obviously mark a specific functional network different from those involving the other components of the electrophysiological response.

To recapitulate the spatio-temporal organization of the gamma effects, Mooney face stimuli triggered a distributed network of gamma responses characterized by: (a) an early burst before 200 ms in the fusiform gyrus and the adjacent lateral occipital cortex, immediately followed by (b) a posterior–anterior propagation along the intra-parietal sulcus, simultaneous with (c) a deactivation in the primary visual cortex.

While the temporal organization of this network cannot be compared with previous studies, its spatial organization is very consistent with prior fMRI findings. Perceived faces elicited a stronger gamma response in specific locations within the ventral occipito-temporal cortex, the lateral occipital cortex, and the intraparietal sulcus. The temporo-occipital cortical sites matched locations found to be more active in fMRI for identified vs. unidentified faces in a identification protocol very similar to ours (Grill-Spector, 2003). Perceived faces, which tend to grab the attention of the viewer, triggered stronger gamma responses in a portion of the intraparietal sulcus (IPS) found to be involved during spatial attention (Rushworth et al., 2001) (see also Fries et al., 2001); and, inverted, but perceived faces, triggered the strongest gamma response in another portion of the IPS that activated during mental rotation (Gauthier et al., 2002). Alternatively, those parietal activations may correspond to the generation of small eye movements: the parietal lobe is involved in the generation of reflex guided saccades, especially in the parietal eye field. It is therefore possible that between two stimuli, the gaze slowly and slightly drifts away from its central fixation, and in such a case, the detection of a meaningful visual stimuli (the detected face) would likely trigger a reflex saccade to bring the image back on the fovea. However, such saccades would have to be very small since we discarded the trials in which traces of eye movements could be seen in the electroocculogram.

The gamma 'deactivation' in the primary visual areas may be less straightforward to understand; however, a general inhibition of the primary visual cortex during high-order processing of complex objects has recently been reported with fMRI (Murray et al., 2002). Since our electrodes did not record from the representation of the central visual field, but from its periphery in the upper field (see Table 2), one possibility is that this deactivation corresponds to a reflex inhibition of the surround when a small image is flashed in the center of the visual field. An interesting alternative is that this deactivation may in fact be global, and not just peripheral, and be the basis for the attentional blink phenomenon.

A unique approach for human brain mapping

With a few other studies (Crone et al., 1998; Howard et al., 2003; Lachaux et al., 2000; Sederberg et al., 2003), this paper strongly advocates that the systematic mapping of all the components of the electrophysiological response, in human intracranial recordings during cognitive tasks, is a necessary step in our understanding of human cognition. It complements nicely (a) approaches that solely focus on the evoked potentials, since those cannot reveal most of the modulations of the EEG or MEG spectrum and (b) the fMRI or PET measures that do not capture the fast dynamics and the multidimensionality of the electrophysiological response. Such a 'time-frequency mapping' is likely to reveal new components of the large-scale networks mediating perception and cognition in general, which are out of the reach of the more classic human brain mapping approaches.

Acknowledgments

The authors wish to thank Dr D. Hoffmann for the placement of intracerebral electrodes and the technical staff in Grenoble's hospital in the Neurology Department, Valérie Balle, Carole Chatelard, Eliane Gamblin, and Anne Thiriaux for continuous and invaluable help. J.P.Lachaux was supported by a grant from the Fyssen foundation.

References

Allison, T., Ginter, H., McCarthy, G., Nobre, A.C., Puce, A., Luby, M., Spencer, D.D., 1994a. Face recognition in human extrastriate cortex. J. Neurophysiol. 71, 821–825.

Allison, T., McCarthy, G., Nobre, A., Puce, A., Belger, A., 1994b. Human extrastriate visual cortex and the perception of faces, words, numbers, and colors. Cereb. Cortex 4, 544–554.

Allison, T., Puce, A., Spencer, D.D., McCarthy, G., 1999. Electrophysiological studies of human face perception: I. Potentials generated in occipitotemporal cortex by face and non-face stimuli. Cereb. Cortex 9, 415–430.

Crone, N.E., Miglioretti, D.L., Gordon, B., Lesser, R.P., 1998. Functional mapping of human sensorimotor cortex with electrocorticographic spectral analysis: II. Event-related synchronization in the gamma band. Brain 121 (Pt. 12), 2301–2315.

Fries, P., Reynolds, J.H., Rorie, A.E., Desimone, R., 2001. Modulation of oscillatory neuronal synchronization by selective visual attention. Science 291, 1560–1563.

Gauthier, I., Hayward, W.G., Tarr, M.J., Anderson, A.W., Skudlarski, P., Gore, J.C., 2002. BOLD activity during mental rotation and viewpoint-dependent object recognition. Neuron 34, 161–171.

George, N., Jemel, B., Fiori, N., Renault, B., 1997. Face and shape repetition effects in humans: a spatio-temporal ERP study. NeuroReport 8, 1417–1423.

Gray, C.M., 1999. The temporal correlation hypothesis of visual feature integration: still alive and well. Neuron 24, 31–47, 111–125.

Grill-Spector, K., 2003. The functional organization of the ventral visual pathway and its relationship to object recognition. In: Kanwisher, N., Duncan, J. (Eds.), Functional Neuroimaging of Visual Cognition. Attention and Performance XX. Oxford Univ. Press, Oxford, pp. 169–193.

Halgren, E., Baudena, P., Heit, G., Clarke, J.M., Marinkovic, K., Chauvel, P., Clarke, M., 1994a. Spatio-temporal stages in face and word processing: 2. Depth-recorded potentials in the human frontal and Rolandic cortices. J. Physiol. (Paris) 88, 51–80.

Halgren, E., Baudena, P., Heit, G., Clarke, J.M., Marinkovic, K., Clarke, M., 1994b. Spatio-temporal stages in face and word processing: I. Depth-recorded potentials in the human occipital, temporal and parietal lobes [corrected]. J. Physiol. (Paris) 88, 1–50.

Haxby, J.V., Hoffman, E.A., Gobbini, M.I., 2000. The distributed human neural system for face perception. Trends Cogn. Sci. 4, 223–233.

Howard, M.W., Rizzuto, D.S., Caplan, J.B., Madsen, J.R., Lisman, J., Aschenbrenner-Scheibe, R., Schulze-Bonhage, A., Kahana, M.J., 2003. Gamma oscillations correlate with working memory load in humans. Cereb. Cortex 13, 1369–1374.

Kanwisher, N., McDermott, J., Chun, M.M., 1997. The fusiform face area: a module in human extrastriate cortex specialized for face perception. J. Neurosci. 17, 4302–4311.

Klopp, J., Halgren, E., Marinkovic, K., Nenov, V., 1999. Face-selective spectral changes in the human fusiform gyrus. Clin. Neurophysiol. 110, 676–682.

Klopp, J., Marinkovic, K., Chauvel, P., Nenov, V., Halgren, E., 2000. Early widespread cortical distribution of coherent fusiform face selective activity. Hum. Brain Mapp. 11, 286–293.

Lachaux, J.P., Rodriguez, E., Martinerie, J., Adam, C., Hasboun, D., Varela, F.J., 2000. A quantitative study of gamma-band activity in human intracranial recordings triggered by visual stimuli. Eur. J. Neurosci. 12, 2608–2622.

Lachaux, J.P., Lutz, A., Rudrauf, D., Cosmelli, D., Le Van Quyen, M., Martinerie, J., Varela, F., 2002. Estimating the time-course of coherence between single-trial brain signals: an introduction to wavelet coherence. Neurophysiol. Clin. 32, 157–174.

Lachaux, J.P., Chavez, M., Lutz, A., 2003. A simple measure of correlation across time, frequency and space between continuous brain signals. J. Neurosci. Methods 123, 175–188.

McCarthy, G., Puce, A., Belger, A., Allison, T., 1999. Electrophysiological studies of human face perception: II. Response properties of face-specific potentials generated in occipitotemporal cortex. Cereb. Cortex 9, 431–444.

Mooney, C.M., 1956. Closure with negative after-images under flickering light. Can. J. Psychol. 10, 191–199.

Murray, S.O., Kersten, D., Olshausen, B.A., Schrater, P., Woods, D.L., 2002. Shape perception reduces activity in human primary visual cortex. Proc. Natl. Acad. Sci. U. S. A. 99, 15164–15169.

Puce, A., Allison, T., McCarthy, G., 1999. Electrophysiological studies of human face perception: III. Effects of top-down processing on face-specific potentials. Cereb. Cortex 9, 445–458.

Rodriguez, E., George, N., Lachaux, J.P., Martinerie, J., Renault, B., Varela, F.J., 1999. Perception's shadow: long-distance synchronization of human brain activity. Nature 397, 430–433.

Rushworth, M.F., Paus, T., Sipila, P.K., 2001. Attention systems and the organization of the human parietal cortex. J. Neurosci. 21, 5262–5271.

Sederberg, P.B., Kahana, M.J., Howard, M.W., Donner, E.J., Madsen, J.R., 2003. Theta and gamma oscillations during encoding predict subsequent recall. J. Neurosci. 23, 10809–10814.

Singer, W., 1999. Neuronal synchrony: a versatile code for the definition of relations? Neuron. 24, 49–65, 111–125.

Tallon-Baudry, C., Bertrand, O., 1999. Oscillatory gamma activity in humans and its role in object representation. Trends Cogn. Sci. 3, 151–162.

Tallon-Baudry, C., Bertrand, O., Delpuech, C., Permier, J., 1997. Oscillatory gamma-band (30–70 Hz) activity induced by a visual search task in humans. J. Neurosci. 17, 722–734.